

Demodulation of Underwater OFDM Transmissions by Time Reversal and Basis Pursuit Methods

João Gomes
Institute for Systems and Robotics
Instituto Superior Técnico
1049-001 Lisboa, Portugal
jpg@isr.ist.utl.pt

Christian R. Berger
Dept. of Electr. & Comp. Engineering
Carnegie Mellon University
Pittsburgh, PA 15213, USA
crberger@ece.cmu.edu

António Silva
SiPLAB — Universidade do Algarve
Campus de Gambelas
8005-139 Faro, Portugal
asilva@ualg.pt

Abstract—In this paper we discuss a channel shortening approach based on passive time reversal (PTR) for underwater acoustic communication using OFDM. PTR exploits the physics of acoustic propagation to mitigate intersymbol interference in a simple and robust way, reducing the need for long OFDM symbols and prefixes. We adopt recent basis pursuit methods for identification of sparse responses from PTR channel probes. This effectively discards unstable or insignificant estimated channel coefficients, improving the performance relative to PTR with directly observed channel responses. We present results for data collected during the CALCOM'10 sea trial with 4.5 kHz bandwidth, 4.1–6.4 kbit/s raw data rates (2–3.2 kbit/s before convolutional coding), and 3 km communication range. Channel responses are sparse, with delay spreads of 20–30 ms that PTR reduces to 5–10 ms. Subsequent OFDM demodulation attains good results in much of the signal bandwidth, although some seemingly source-related issues remain that lead to overall higher error rates than using plain OFDM with multichannel combining.

I. INTRODUCTION

Multicarrier modulation, particularly orthogonal frequency-division multiplexing (OFDM), has recently attracted much attention in underwater acoustic (UWA) communications [1]–[4], as an alternative to conventional single-carrier systems, where time-domain equalizers are used at the receiver [5]. In spite of their being regarded as a nearly standard solution for high-rate coherent communication, equalization-based receivers are rather sensitive to the choice of filter lengths and other parameters, leading to somewhat inconsistent demodulation performance in practice. By contrast, the parameters of plain FFT-based receivers used in OFDM are simpler to adjust, and the spectral flexibility of this technique also provides useful degrees of freedom for coding and to adapt the waveform to channel conditions.

The biggest drawback of OFDM in UWA applications is perhaps the requirement that long enough prefixes to symbols (zero or cyclic prefixes) be adopted to encompass most of the channel intersymbol interference (ISI). To maintain a reasonable efficiency this might call for very long OFDM symbols, which raises other problems such as enhanced sensitivity to channel variations due to narrow spacing of carriers. The above shortcomings may be addressed by intentionally limiting the symbol and prefix lengths, and endowing OFDM receivers with more sophisticated equalizers to remove interblock in-

terference (IBI) or intercarrier interference (ICI) [6], [7]. However, this brings back to some extent the parametrization issues of equalizers for single-carrier systems.

In some of the reported UWA OFDM experiments channel impulse responses are quite favorable, lasting for less than 10 ms. Reasonably short cyclic prefixes and guard intervals can therefore be used. However, questions naturally arise regarding the suitability of OFDM for general-purpose modems that must also operate in severely dispersive UWA channels, with impulse responses spanning several tens of milliseconds. In this work we explore a prefiltering approach (channel shortening) to mitigate ISI through passive time reversal (PTR) [8], so that moderate lengths for prefixes and OFDM symbols can be used without additional complications [9], [10]. This technique synthetically emulates a physical property of propagation in a waveguide — time reversal, or phase conjugation — that can be used to refocus signals in time and space originating at a point source, with no environmental information, if the distorted signals observed at a set of receivers are time-reversed and retransmitted. The main advantage of PTR is simplicity, as all that is required for synthetic backpropagation is readily obtained from the received signals. The drawback is that a relatively long and dense array of receivers is needed to sample the acoustic field in the water column. This requirement may be relaxed in communications applications, where the receiver has the ability to handle some residual ISI from the PTR preprocessor.

In its basic form, PTR uses observed channel probes, which are then time-reversed and convolved with the packet to emulate backpropagation in the waveguide [11]. Under moderate to low SNR the noise present in the probe is carried over to the output through convolution, degrading the quality of the time-reversed signal and of the estimated symbols in the packet. An alternative is to estimate the channel response by system identification techniques from a known part of the transmitted signal [11]. In this work we adopt basis pursuit (BP) methods [12], which are currently very popular in compressive sensing applications, to estimate channel responses directly from the probes themselves. This avoids the need for dedicated channel probing waveforms that reduce the efficiency of communication, as our linear FM (LFM) probes are used for other purposes such as fine packet synchronization

and coarse Doppler compensation.

The current surge of research interest in BP methods for wireless communications is motivated by the fact that many transmission channels exhibit sparse responses, and improvements in efficiency (e.g., fewer training data) or performance may be obtained by exploiting this property [13]–[15]. In UWA communications sparsity has also been successfully exploited through coefficient truncation to reduce the output mean-square error (MSE) of adaptive receivers by discarding small and jitter-prone estimated channel coefficients [16], [17].

We adopt SpaRSA [18] as a solver for ℓ_2 - ℓ_1 BP, where a least-squares (LS) cost function is augmented with the scaled ℓ_1 norm of the desired coefficient vector. The presence of the ℓ_1 term tends to set to zero nearly irrelevant coefficients, yielding a sparse “skeleton” of the impulse response containing much less noise than in other methods used for PTR. This type of sparsification approach provides more reliable results than simple coefficient truncation by setting a threshold on coefficient magnitudes, albeit at a cost of increased computational load. Transmission rates in UWA channels are sufficiently low that this approach does not seem far-fetched for real-time operation given the current state of technology [19]. SpaRSA can natively handle complex signals so, unlike other popular ℓ_2 - ℓ_1 methods, it directly operates on baseband waveforms.

The experimental data for this work was collected during the CALCOM’10 sea trial, that was conducted off the south coast of Portugal on June 22–24, 2010. The communication range varied from about 300 m to 3 km, over a mildly variable water depth of 100–200 m. The arrival wavefront structure at the array is clearly visible at the 16-hydrophone receiver array, with strong direct and surface-reflected paths, and weaker bottom and bottom-surface bounces. The delay spread is on the order of 20–30 ms.

Several different modulation formats were transmitted with bandwidths of 4.5 kHz or 7.5 kHz. In this work we examine OFDM packets with 4.5 kHz bandwidth and 5.5 kHz carrier frequency. We compare the performance of TR+OFDM (single-channel OFDM demodulation with PTR preprocessing) with the more popular multichannel combining approach (MC-OFDM), where channel responses are estimated from OFDM pilots at individual array sensors, and combined to produce more reliable symbol estimates [1]. We also assess the impact of BP-estimated vs. observed channel probes, and benchmark the performance of OFDM against equalization-based demodulation of QPSK packets with similar spectral efficiency.

II. CHANNEL SHORTENING USING PASSIVE TIME REVERSAL

Active time reversal is a technique for wave focusing in propagation media that resorts to feedback to circumvent the need for detailed environmental knowledge at the focusing device. As depicted in Fig. 1 a point source first transmits a signal to the time-reversal (TR) array which, ideally, fully intersects the acoustic field propagating in the waveguide,

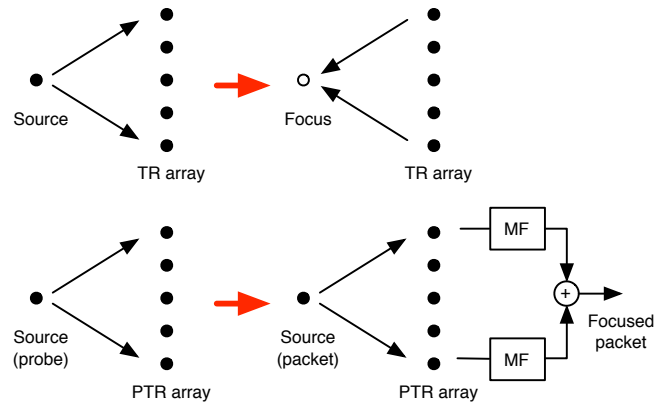


Fig. 1. Illustration of active and passive time reversal

recording distorted signals at each point. By replaying those signals reversed in time the TR array is able to automatically refocus an undistorted (but time-reversed) replica of the original transmission at the source location.

PTR, also shown in Fig. 1, emulates this physical process synthetically. The source first transmits a channel probe, followed by a data packet. The PTR array stores the distorted probes, time-reverses them, convolves them with the received packet replicas, and sums to regenerate a distortionless packet. In practice linear and relatively sparse PTR arrays are used, and the departure from ideal conditions precludes the full elimination of multipath after synthetic time reversal. Still, practical PTR is able to create an equivalent point-to-point channel whose impulse response is significantly more concentrated than any of the individual source-to-sensor responses, and is thus useful for effectively shortening the channel. That is the key property exploited in our work.

We denote the baseband complex transmitted probe by $p(t)$ and the transmitted packet by $x(t)$. Their baseband distorted received replicas at the m -th hydrophone of the PTR array are $h_m(t)$ and $y_m(t)$, respectively. For source-to-hydrophone impulse response $g_m(t)$ these are related by the convolutions

$$h_m(t) = g_m(t) \star p(t), \quad y_m(t) = g_m(t) \star x(t). \quad (1)$$

The PTR output is given by

$$z(t) = \sum_{m=1}^M \hat{g}_m^*(-t) \star y_m(t), \quad (2)$$

where $\hat{g}_m(t)$ is an estimate of $g_m(t)$. For pulse compression of observed probes, e.g., we have $\hat{g}_m(t) = h_m(t) \star p^*(-t)$, hence

$$z(t) = r(t) \star \gamma(t) \star x(t), \quad (3)$$

$$\gamma(t) \triangleq \sum_{m=1}^M g_m^*(-t) \star g_m(t), \quad r(t) \triangleq p(t) \star p^*(-t). \quad (4)$$

For properly designed probes, such as the LFM signals used in the CALCOM’10 experiment, the spectrum of the probe autocorrelation function $r(t)$ is nearly constant across the signal bandwidth and can be eliminated from (3). Similarly,

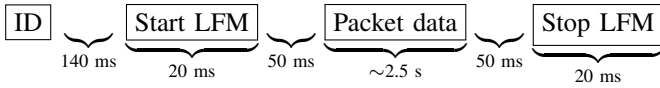


Fig. 2. CALCOM'10 packet structure

successful time reversal yields a medium autocorrelation function $\gamma(t)$ whose spectrum varies much less than any of the spectra of $g_m(t)$ across the signal band. Subsequent receiver algorithms may be able to cope with the residual distortion due to $\gamma(t)$ more easily than if they were directly experiencing the full impact of $g_m(t)$.

III. SIGNAL MODEL FOR THE CALCOM'10 EXPERIMENT

A. Packet Structure

Fig. 2 shows the structure of one CALCOM'10 packet. The packet ID is formed by a sequence of upswing or downswing LFMs spanning the whole signal bandwidth, which encode a unique identifier for each type of packet as a binary number. Start/stop LFM channel probes flanking the data part of each packet also span the whole bandwidth, albeit over a shorter interval. They are used for several purposes, e.g., fine packet synchronization, assessment of packet duration for coarse Doppler compensation, and channel identification.

B. OFDM Signals

The baseband transmitted signal is a superposition of K orthogonal subcarrier waveforms over N OFDM symbols

$$x(t) = \sum_{l=0}^{N-1} \sum_{k=0}^{K-1} a_k(l) e^{j \frac{2\pi k}{T} (t-lT_b)} \Pi\left(\frac{t-lT_b}{T}\right), \quad (5)$$

where $a_k(l)$ denotes a point from the k -th subcarrier complex constellation in the l -th OFDM symbol interval, T is the basic OFDM symbol duration given by the reciprocal of the subcarrier frequency spacing, $T_b = T + T_g$ is the total symbol duration including an appended guard interval T_g , and Π is a rectangular pulse shape

$$\Pi(t) = \begin{cases} 1, & 0 \leq t < 1 \\ 0, & \text{otherwise.} \end{cases}$$

This model corresponds to zero-padded (ZP) OFDM, where cyclic extensions to symbols are absent. However, in our demodulation algorithms we overlap-add the ZP to the head of each symbol to retain the simplicity of FFT-based processing.

Subcarriers are partitioned into K_g guard subcarriers, K_n null subcarriers, K_p pilot carriers, and K_a active carriers, such that $K = K_g + K_n + K_p + K_a$. To account for non-ideal front-end bandpass filtering $K_g \approx K/10$ guard subcarriers are symmetrically inserted at the lower and upper edges of the signal band. Null, or virtual, subcarriers are spread throughout the signal band to aid in residual Doppler estimation. Null symbols are inserted in both guard and null subcarriers. In our experiment pilots are not explicitly inserted, but rather chosen as needed from the known contents of each packet. Typically $K_p \approx K/4$ pilots, uniformly spaced across the signal band, are used for channel estimation.

All OFDM signals are processed in baseband, sampled at a rate equal to (an integer multiple of) the signal bandwidth.

C. Generation, Coding, and Mapping of Packet Bits

Packet data are generated by truncating a pseudorandom bit sequence, built from a M-sequence of length $2^{15} - 1$, applying convolutional coding, interleaving, and mapping to (subcarrier) QPSK constellations. We adopt a widely used convolutional code with rate 1/2, constraint length 7, octal generator polynomials (133; 171), and no puncturing [20, Tab. 8.3-1].

For code rate 1/2, K_a active carriers, N OFDM symbols, and 2 bits per QPSK constellation point used in each subcarrier, a total of $K_a N$ bits are needed at the input of the convolutional encoder. The processing steps are as follows:

- 1) Read $K_a N$ input bits from the M-sequence.
- 2) Convolutionally encode the bit sequence to get a stream of $2K_a N$ coded bits.
- 3) Partition into N blocks of length $2K_a$ that will be used to generate each OFDM symbol.
- 4) Randomly interleave each block (subcarrier dimension). There is no interleaving across OFDM symbols (time dimension).
- 5) Map consecutive pairs of bits to QPSK constellation symbols.

The redundancy of coding in CALCOM'10 is much lower than that of a BCH(64,10) code that has been reported in several UWA OFDM communication experiments [21], but it does achieve decoding with low bit error rates for good receiver architectures.

IV. RECEIVER ALGORITHMS

A. Coarse Doppler compensation

Time-scaling of acoustic waveforms due to transmitter, receiver, or surface motion induces broadband Doppler shifts that are not uniform across OFDM subcarriers. A popular approach for eliminating the dominant Doppler components is to estimate the time compression or dilation of packets by detecting the start/stop probes (Fig. 2), comparing the received vs. transmitted probe-to-probe intervals, and resampling the received signals to undo any compression/dilation [22]. When all path delays in the channel impulse response are varying linearly at the same rate, it was shown in [1] that resampling of an OFDM signal will approximately reduce the Doppler distortion to a residual narrowband component that shifts all carriers uniformly. Moreover, for typical values of the time scaling factor close to 1 the resampling operation on packets/probes will not compromise the ability of passive time reversal to mitigate ISI in refocused signals [11]. A single average scaling factor is used for resampling across all hydrophone signals.

B. Channel Identification for Passive Time Reversal

In its simplest form a PTR processor uses observed (and possibly pulse-compressed) channel probes, conjugated and reversed in time, as templates for convolution with packet

data waveforms. As shown in the results in Sec. V, observed probes are noisy and may lead to performance loss in OFDM demodulation through the introduction of convolutional noise at the output of PTR. Alternatively, system identification techniques may be used to obtain a less noisy channel estimate, but the short duration of probes (20 ms in CALCOM'10) relative to the expectable impulse response duration suggests that additional properties, such as sparsity, should be exploited to improve the accuracy of these estimates.

Recent achievements in compressive sensing (CS) have sparked enormous interest for solving various linear, but ill-posed, inverse problems, where sparsity acts as a regularization criterion to stabilize the solution [12]. Several applications of CS in channel identification for wireless communications have been proposed, although in this setting ill-posedness is not necessarily an issue, and sparsity may only play the role of a convenient feature that reduces the number of effective degrees of freedom, yielding faster and more precise solutions.

For each hydrophone we wish to identify a vector \mathbf{g} of impulse response coefficients, $g_m(n_{g-}), \dots, g_m(n_{g+})$, from a block of observed probe samples, $h_m(n_{h-}), \dots, h_m(n_{h+})$, stacked in vector \mathbf{h} . Conventionally, a LS problem in block or recursive form is solved to obtain \mathbf{g} given \mathbf{h} and knowledge of the transmitted waveform. In BP identification we solve an extended ℓ_2 - ℓ_1 optimization problem of the form

$$\min_{\mathbf{g}} \frac{1}{2} \|\mathbf{h} - \mathbf{P}\mathbf{g}\|_2^2 + \tau \|\mathbf{g}\|_1, \quad (6)$$

where the first term coincides with the above LS criterion, while the second one is a regularizer which acts as a surrogate for the intractable ℓ_0 norm, and tends to penalize more heavily vectors \mathbf{g} with many nonzero components. The regularization parameter τ controls the relative weight of the two terms, hence the level of sparsity in the solution, and as a rule of thumb should be chosen on the order of magnitude of the ℓ_2 norm of the columns of matrix \mathbf{P} . This is a dictionary (convolution) matrix with delayed replicas of the sampled transmitted LFM pulse, padded with leading/trailing zeros as necessary.

We use SpaRSA as a solver for (6) [18]. SpaRSA is a general framework for numerically solving unconstrained optimization problems with cost function $f(\mathbf{g}) + \tau c(\mathbf{g})$, where f is a smooth function and c is the sparsity-inducing regularizer which, in state of the art CS methods, is nonquadratic and nonsmooth. For the ℓ_1 regularizer in (6) SpaRSA repeatedly evaluates simple so-called *soft threshold* functions that transparently clip small entries in the real or complex coefficient vector to exactly zero. Currently, SpaRSA is competitive with the fastest known numerical methods for the standard ℓ_2 - ℓ_1 problem, among others.

SpaRSA does not manipulate the dictionary matrix directly, but only through products $\mathbf{P}\mathbf{g}$, $\mathbf{P}^H\mathbf{h}$ that can often be computed efficiently even for very large problem sizes. This is the case for our dictionary, where \mathbf{P} is not explicitly built, but rather the products are evaluated by convolving h_m , p , or g_m using FFT/IFFT operations. The impulse-like autocorrelation

function of LFM probes means that the columns of \mathbf{P} are nearly orthogonal, and this translates into fast convergence of SpaRSA.

Solving (6) does not lead to a LS solution for \mathbf{g} over the set of identified nonzero taps. SpaRSA provides an optional postprocessing step known as *debiasing*, where a true LS solution is calculated, restricted to the set of dictionary entries where nonzero coefficients were identified during the main processing phase. In spite of its efficiency, debiasing can account for a large fraction of the processing time in SpaRSA, and was not used.

C. OFDM CFO estimation

After coarse Doppler compensation by resampling, some residual components remain due to differential Doppler and scaling factor estimation error. The latter manifests itself as a uniform shift of all subcarriers, known as carrier frequency offset (CFO), and is compensated here by the same virtual subcarrier (VSC) method used in [1]. In this method the energy in non-guard null carriers is evaluated for each OFDM symbol using a grid of possible Doppler shifts by multiplying the time-domain signal with suitable complex exponentials, and the one leading to lower total energy in that set of subcarriers is selected.

D. OFDM channel estimation

Pilot subcarriers for OFDM channel estimation are uniformly spaced across the signal bandwidth, excluding guard bands. Let $k_{p_1}, \dots, k_{p_{N_p}}$ denote the indices for N_p pilot carriers that are integer multiples of the carrier spacing factor ΔK . Similarly to (6) we model the pertinent channel response as a set of coefficients $g(n_{g-}), \dots, g(n_{g+})$, where $n_{g-} < 0$ reflects the presence of precursors (particularly relevant after PTR, which synthesizes an equivalent response that is approximately symmetric around delay zero). We build a DFT matrix of size N_p , and select columns n_{g-}, \dots, n_{g+} , modulo N_p , to form submatrix \mathbf{A} . We find the channel coefficient vector \mathbf{g} as the solution of

$$\min_{\mathbf{g}} \|\mathbf{b} - \mathbf{A}\mathbf{g}\|^2, \quad (7)$$

where \mathbf{b} is the vector of measured channel gains for the pilot subcarriers (i.e., FFT outputs divided by the known pilot symbols), reordered according to $k_{p_1}/\Delta K, \dots, k_{p_{N_p}}/\Delta K$ modulo N_p . The desired channel gains for frequency-domain OFDM equalization are obtained by zero-padding sequence g , taking its FFT of size $N_p\Delta K$, and extending its values, modulo $N_p\Delta K$, to the full set of subcarrier indices $0, \dots, K$. This procedure interpolates the channel frequency response between pilot carriers and periodically extends it to the upper and lower guard bands, thus removing the ill-posedness of estimation due to lack of channel measurements in these bands.

In MC-OFDM the k -th active carrier is processed by stacking the interpolated channel gains, G , for the set of M (or less) hydrophone signals, as well as the observed FFT outputs, Y , yielding a vector linear model for the unknown constellation

symbol

$$\begin{bmatrix} Y_{1k} \\ \vdots \\ Y_{Mk} \end{bmatrix} = \begin{bmatrix} G_{1k} \\ \vdots \\ G_{Mk} \end{bmatrix} a_k + \mathbf{w}_k, \quad (8)$$

where \mathbf{w}_k denotes a noise vector. Symbol a_k is then given by the LS solution of (8).

Processing the received signals in individual hydrophones, as in MC-OFDM, requires that they be properly aligned in time. In CALCOM'10 this may be done by detecting the packet start probe at each hydrophone and delaying/advancing the main packet waveform accordingly. This is not an issue in PTR, as the convolution with time-reversed probes automatically provides temporal alignment before adding the signals.

E. Decoding of Packet Bits

Unmapping of packet bits reverses the operations described in Sec. III-C:

- 1) Use the FFT outputs for null/guard carriers to estimate the (white and Gaussian) noise power.
- 2) Compute soft estimates for 2 bits in each active subcarrier as the log-likelihood ratio (LLR) of 1/0 values given the observed subcarrier symbol estimate.
- 3) Randomly deinterleave soft bits along the subcarrier dimension, and concatenate for all OFDM symbols in the packet.
- 4) Use a soft-input Viterbi algorithm to decode the convolutional code [20], retrieving the final bit sequence.

V. EXPERIMENTAL RESULTS

The CALCOM'10 sea trial was conducted south of Faro, Portugal, on June 22–24, 2010. The test area was approximately 3×3 km² at $36^\circ 52'$ N, $8^\circ 3.8'$ W, with bottom sloping along the NE/SW direction from 100 to 200 m. Bottom sediments at the site are silty, with an estimated compressional sound propagation speed of 1550 m/s. The sound speed profile (SSP) in the water column is downward refracting, decreasing from 1514 m/s at the surface to 1507 m/s at 60 m, and remaining approximately constant below that. The receiver was a vertical drifting array with 16 uniformly-spaced hydrophones from 6 m to 66 m depth.

The signals analyzed here were transmitted with carrier frequency 5.5 kHz and bandwidth 4.5 kHz using a Lubell LL-1424HP source at 10 m depth. Tab. I summarizes the parameters for three different types of OFDM packets denoted by O1–3, each lasting for about 2.5 s.

A. Channel Responses

We focus on transmissions at 3.1 km range on June 24. Fig. 3 shows pulse-compressed received probes for one of the packets, BP-estimated channel responses using (6), and predictions using the Bellhop ray tracer with available GPS data, bathymetry, and SSP measurements. The deepest hydrophone signals (#16) were discarded due to hardware problems. The wavefront structure of the acoustic field impinging upon the receiver array is clearly visible in these plots. They show a

TABLE I
OFDM SIGNAL PARAMETERS IN THE CALCOM'10 EXPERIMENT

Packet type	O1	O2	O3
Bandwidth [kHz]	4.5		
Subcarriers K	128	256	512
Carrier spacing [Hz]	35.2	17.6	8.8
Active interval T [ms]	28.4	56.9	113.8
Guard interval T_g [ms]	25		
In-band null carriers K_n	5	10	20
Guard carriers K_g	6+7	13+13	25+26
Number of symbols N	47	31	18
Constellation	QPSK		

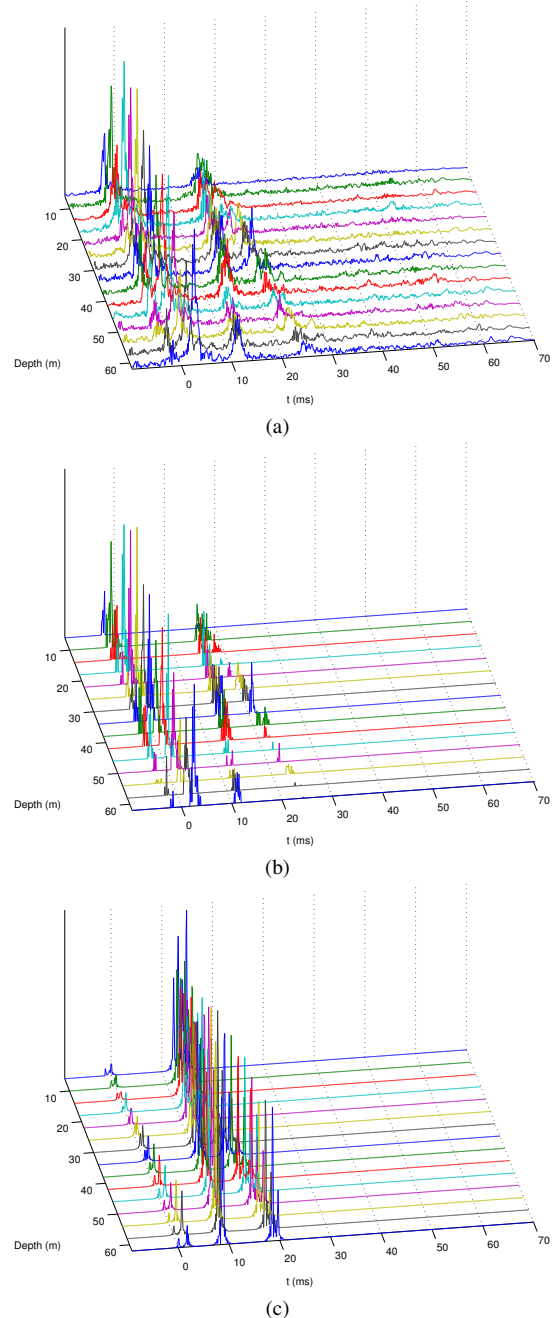


Fig. 3. Estimated channel responses (a) Pulse-compressed probes (b) Basis pursuit (c) Simulation

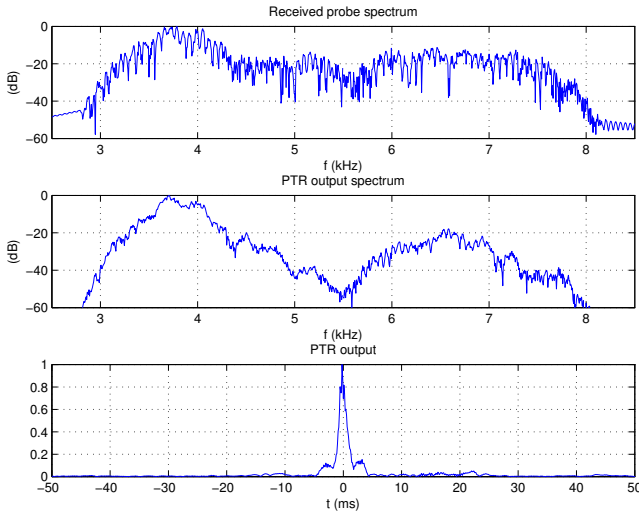


Fig. 4. Time reversal of channel probes, showing the spectrum of a received (stop) LFM probe at hydrophone #7, and the PTR output signal in the frequency and time domains

closely-spaced direct arrival and surface bounce with delay dispersion of up to about 5 ms at the bottom hydrophone, followed by a bottom bounce with 10–15 ms delay and a bottom-surface bounce with up to 25 ms delay. Experimental results are in good agreement with simulated data, although the bottom-interacting arrivals are weaker than predicted by the ray tracer. This makes the interpretation of results more reliable than in our previous OFDM transmission experiments [9], [10].

BP estimation successfully retrieves the “skeleton” of the multipath, while setting to zero most of the estimated coefficients. Both the LFM template and multichannel received probes, sampled at 9 kHz, were pre-normalized for unit maximum magnitude, the dictionary matrix spanned delays of -10 ms to 70 ms, and the regularization parameter was set to $\tau = 4.5$. Under these conditions SpaRSA runs 30–35 iterations per hydrophone, returning a vector with about 30 nonzero coefficients.

B. Time Reversal of Channel Probes and QPSK Packets

The availability of a pair of channel probes flanking each packet, spaced by more than 2.5 s, provides a simple means to test the performance of PTR over a relatively large horizon. Here, start LFMs act as channel probes and stop LFMs as packet data. Fig. 4 shows the spectra of a received (stop) LFM probe at hydrophone #7 and of the PTR output, as well as the corresponding time-domain signal. PTR attains significant concentration of energy around delay zero, but the spectrum of the refocused probe remains quite distorted. For comparison, Fig. 5 shows similar results for simulated data under the conditions of Fig. 3c, where the output spectrum is seen to be much flatter across the signal band, as one would expect for the factor γ in (3). The discrepancy is due to the fact that, although some of the simulated hydrophone signals also exhibit strong attenuation across broad intervals

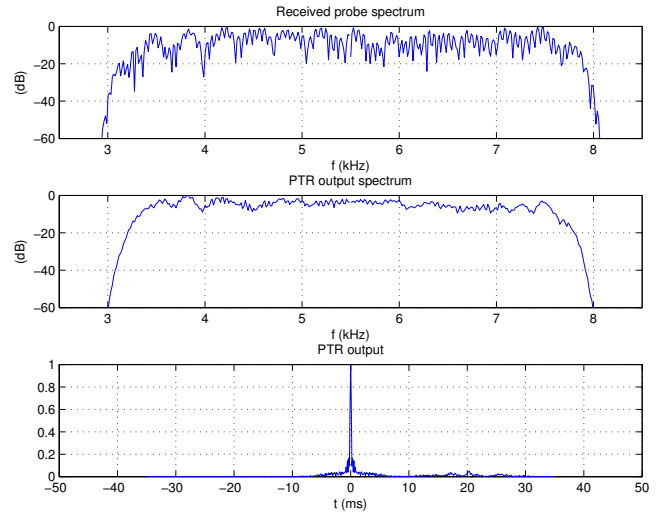


Fig. 5. Time reversal of channel probes (simulation counterpart of Fig. 4 under the conditions of Fig. 3c)

TABLE II
QPSK SIGNAL PARAMETERS IN THE CALCOM’10 EXPERIMENT AND SAMPLE DEMODULATION PERFORMANCE

Packet type	Q1	Q2	Q3
Bandwidth [kHz]		4.5	
Symbol rate [baud]	2250	2812.5	3214.3
Rolloff	1	0.6	0.4
Number of symbols	5625	7031	8036
Constellation	QPSK		
MDFE MSE [dB]	-13.8	-12.9	-13.1
TR+DFE MSE [dB]	-14.2	-13.5	-11.9

of the signal bandwidth, there is sufficient diversity of spectral behavior in different hydrophone signals for the PTR spectrum to become reasonably flat. In the experimental data, however, strong fading is observed in all hydrophones between 4.5 kHz and 6 kHz, and by essentially squaring the magnitudes of spectra and summing across hydrophones PTR contributes to exacerbate this imbalance. So, while the PTR output spectrum of Fig. 4 definitely shows fewer short-term variations with frequency, the disparity of magnitudes over the signal band may be problematic. Broad fading as shown in Fig. 4 could be caused by interference between two received signal replicas with similar magnitudes spaced by a fraction of a millisecond (about 3–4 samples at our baseband sampling frequency of 9 kHz), but consistently observing this phenomenon across all hydrophones suggests that it may be a feature of the transmitted signal, rather than of the propagation medium. At present the question of whether the source is actually causing this distortion remains open.

To provide a counterpoint for OFDM demodulation we also present some results for demodulation of QPSK packets in Fig. 6 and the bottom of Tab. II. We examine receiver architectures using full multichannel decision-feedback equalization with 4 of the hydrophone signals (MDFE), as well as PTR followed by a single-channel DFE (TR+DFE). The choices of parameters for QPSK packets (Q1–3), listed in the upper part of Tab.

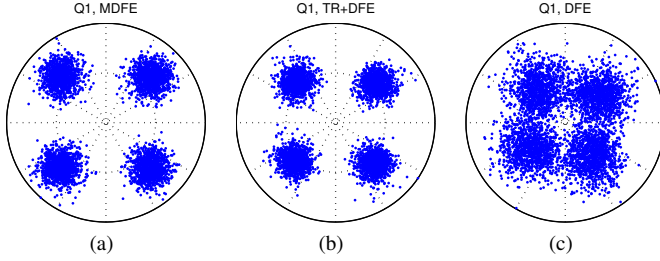


Fig. 6. Sample output constellations for demodulation of QPSK packets (a) Multichannel DFE, hydrophones #2, 6, 10, 14 (b) TR+DFE (c) Single-channel DFE, hydrophone #7

II, are such that Q1, Q2, Q3 have similar spectral efficiency to packets O1, O2, O3, respectively. Hence, results can be compared across modulations in a fair way. The constellation plots of Fig. 6 make it clear that, for equalizer output MSEs of less than -10 dB attained with MDFE and TR+DFE, the raw symbol error rate is practically zero.

The MDFE splits the 2-oversampled input signals from 4 hydrophones into 8 parallel streams sampled at symbol rate. Each stream is processed by a feedforward filter with both causal and anticausal taps, spanning delays (symbol intervals) n_{f-} to n_{f+} . The DFE feedback filter processes the most recent n_b symbol decisions. The triplets (n_{f-}, n_{f+}, n_b) that we use in MDFE for Q1-3 packets are $(-5, 5, 10)$, $(-5, 10, 20)$, and $(-10, 10, 40)$, respectively. For TR+DFE the single-channel DFE uses $(-5, 5, 5)$ for all packet types. These parameters were empirically set by searching for best results on a grid of candidate equalizer lengths. The results show that signal combining by PTR followed by single-channel DFE attains very similar MSE performance to MDFE. Relative to TR+DFE the latter uses fewer hydrophone signals, but the computational complexity of the equalizer is higher (we use a numerically robust QR-RLS algorithm with forgetting factor 0.995). Either of these multichannel combining strategies is required for attaining demodulation with low symbol error rates; for single-hydrophone equalization output MSEs are on the order of -5 dB, and even with perfect feedback of symbol decisions the resulting constellation is much more scattered than for MDFE or TR+DFE (Fig. 6c).

In QPSK packets symbols are spread across all the bandwidth, and enough information content is present in the distorted TR pulse (Fig. 4) for DFEs to estimate those symbols successfully. Note that by using multichannel processing and feedback of previous decisions DFEs don't need to invert the channel for computing symbol estimates [20].

C. Time Reversal of OFDM Packets

Figs. 7 and 8 show the average MSE across subcarriers and the pattern of raw symbol errors in the packet as a function of time (OFDM symbol index) and frequency (subcarrier index) for the proposed TR+OFDM approach, and also for single-hydrophone (#7) OFDM demodulation. The observed behavior for time reversal is consistent with the previous observations for time reversal of probes, i.e., errors

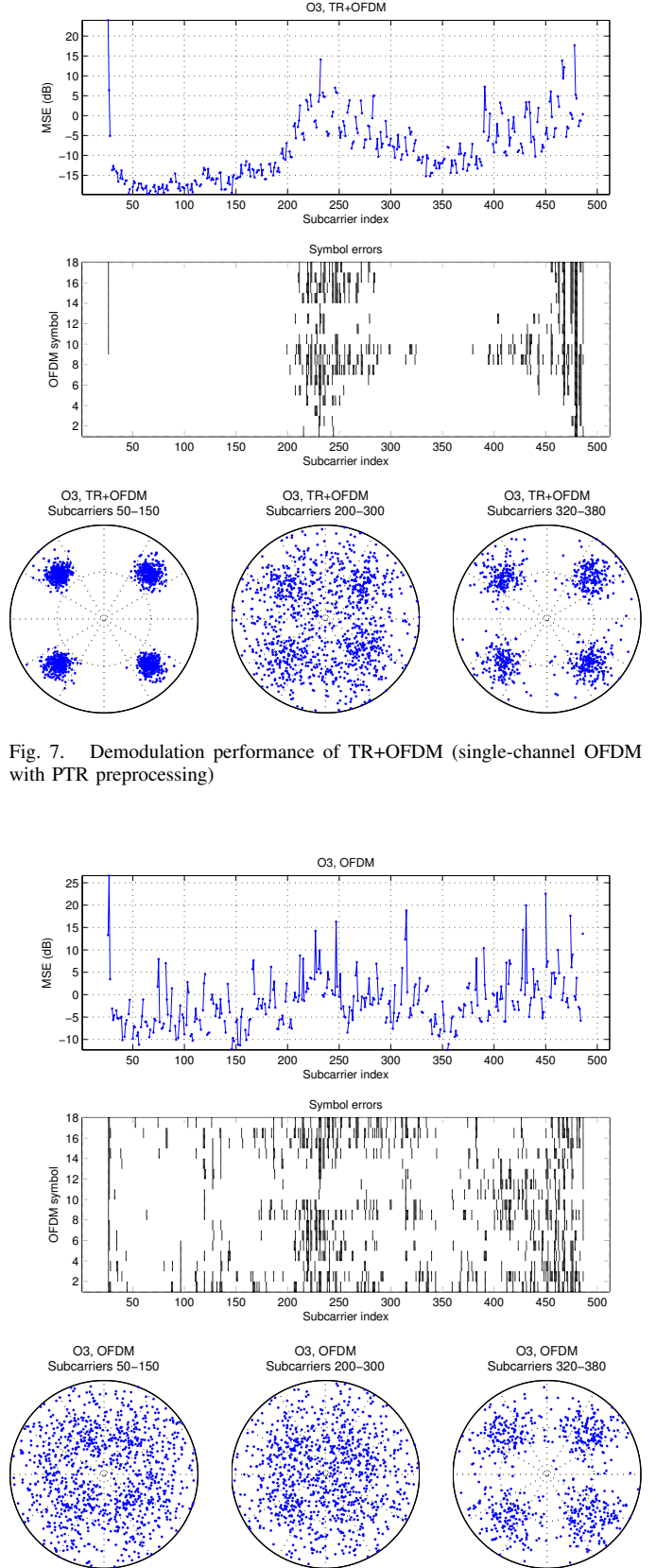


Fig. 7. Demodulation performance of TR+OFDM (single-channel OFDM with PTR preprocessing)

Fig. 8. Demodulation performance of single-channel OFDM (hydrophone #7)

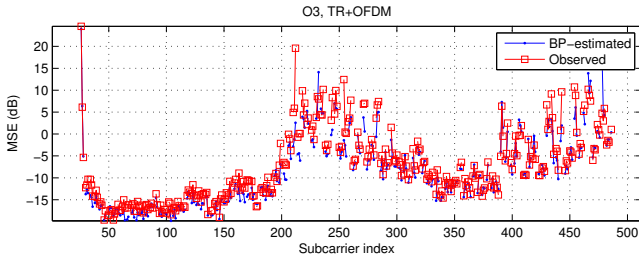


Fig. 9. Performance of TR+OFDM with BP-estimated vs. observed (pulse compressed) probes

are concentrated in “central” frequencies where PTR further attenuates already weak signal components, and also in carriers near the band edges, where the pilot-aided method used for interpolation of channel responses is less accurate. Note that low error rates are obtained in the frequency bands where PTR operates as intended, yielding a strong and relatively flat equivalent response (e.g., 3.5–4.5 kHz). By contrast, errors for single-hydrophone OFDM demodulation in Fig. 8 are more evenly spread across time and frequency, and MSEs tend to be larger and fluctuate more between adjacent carriers. The higher density of errors at the upper signal band when compared to the lower one was observed for all tested OFDM demodulation methods. It could be due to distortions introduced by the acoustic source, whose upper limit of 8 kHz is quite close to the limit of the signal band (7.8 kHz).

Regarding the impact of estimating channel responses using BP methods, as opposed to simply observing pulse compressed probes, Fig. 9 compares the MSE values for both approaches as a function of subcarrier index for the same O3 packet of Figs. 7 and 8. On average, the MSE using BP estimation is 1.2 dB lower than using observed probes (−8.6 dB vs. −7.4 dB), which translates into fewer raw symbol errors (532 vs. 716) and coded bit errors (17 vs. 90).

The results for TR+OFDM in this section, and for TR+DFE above, are obtained by clipping probes outside the delay interval from −5 to 10 ms. This operation is usually done in practical time reversal, as probe components with larger delays are less stable, and coupled with imperfect focusing in sparse arrays tend to introduce long-term echos in the PTR output that end up degrading the performance of ensuing digital receivers.

Figs. 10 and 11 compare the raw symbol error rates and coded bit error rates for MC-OFDM based on (8) and TR+OFDM, as a function of the number of hydrophones used for multichannel combining (starting from the one closest to the surface). For the experimental data under analysis MC-OFDM is clearly superior to TR+OFDM, attaining error-free, or nearly error-free, decoding of bits using only 4 or 5 hydrophones. The reasons for the relatively modest performance of TR+OFDM have already been discussed; however, we note that for the simulated channel of Fig. 3c, which is similar to observed responses, albeit with stronger bottom-interacting arrivals, the situation is reversed. Our simulations indicate that MC-OFDM fails completely in that scenario due to unsuccessful channel identification, whereas TR+OFDM, which does not

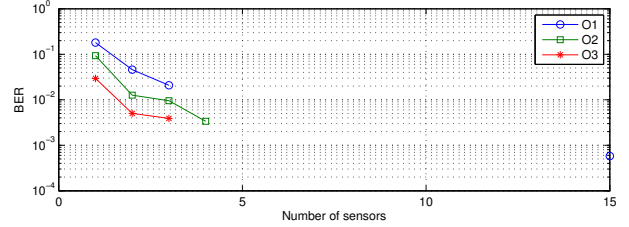
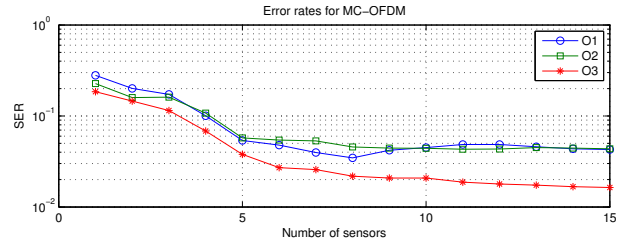


Fig. 10. Raw symbol and coded bit error rates for MC-OFDM

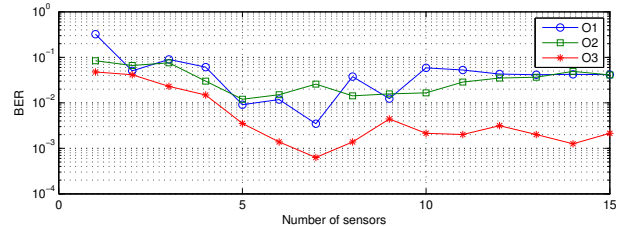
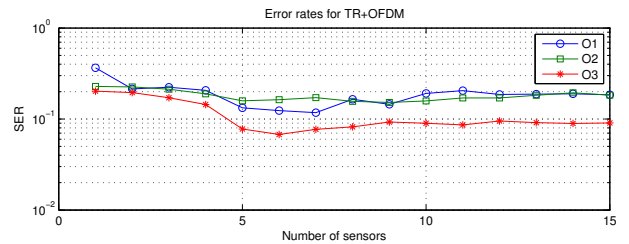


Fig. 11. Raw symbol and coded bit error rates for TR+OFDM

suffer from the observed undesirable systematic attenuation in the middle of the signal band, attains error-free decoding.

Several experiments and simulations have shown that PTR focusing performance tends to saturate as a function of the number of hydrophones, with highest increments being attained for few array sensors [11], [23]. In light of this, and considering the observed superiority of MC-OFDM, as well as its predicted limitations under strong multipath, we tested a hybrid MC/PTR strategy where we (i) partition the 16-element array into several shorter subarrays, (ii) perform PTR processing on each subarray, and (iii) perform OFDM channel estimation and MC combining of the PTR outputs. Tab. III shows that the hybrid approach, using non-overlapping subarrays with 4 hydrophones, yields performance improvements relative to full PTR, and even attains error-free bit decoding in one of the tested packets.

VI. CONCLUSION

In this work we examined OFDM demodulation using PTR preprocessing for underwater communications. The goal

TABLE III
DEMODULATION ERRORS OF PLAIN PTR VS. HYBRID MC/PTR

Packet type	O1	O2	O3
# Active Symbols	3807	5053	5868
# Bits	5170	6820	7938
TR+OFDM			
Raw symbol errors	703	924	532
Coded bit errors	215	279	17
TR+MC-OFDM			
Raw symbol errors	700	821	387
Coded bit errors	185	116	0
MC-OFDM			
Raw symbol errors	163	220	96
Coded bit errors	3	0	0

was to shorten the impulse responses of severely distortive channels to a point where residual ISI could be handled by conventional OFDM techniques without the need for excessively long symbols/prefixes.

Experimental results for CALCOM'10 data confirmed a significant concentration of energy in refocused impulse responses. However, fading over a large fraction of the signal bandwidth was consistently observed over all hydrophones, which deviates from the assumptions of time reversal, exacerbates the attenuation in refocused packets at those frequencies, and leads to symbol errors when demodulating the subcarriers. This is the main factor that explains the observed differences in performance between the proposed TR+OFDM approach and MC-OFDM (i.e., OFDM using multichannel combining). TR+OFDM achieved low error rates at frequencies where consistent fading was not observed. Simulation results suggest that under stronger multipath MC-OFDM may fail due to poor channel identification at individual hydrophones, whereas channel shortening in TR+OFDM still enables successful demodulation.

PTR preprocessing was also successful in single-carrier packets, where the above spectral distortion of refocused signals in part of the bandwidth is less of a concern than in OFDM. An ensuing single-channel DFE with short filter lengths attained essentially the same performance of the best multichannel DFE operating on a subset of 4 hydrophones.

We compared conventional PTR using pulse compressed observed probes with an approach where sparse channel estimates are obtained from received probe signals using BP methods. Sparse estimates retain only the main multipath components, eliminating unstable or insignificant contributions. Decreasing the number of effective impulse response coefficients enabled a reduction in MSE and raw/coded error rates of OFDM packets. The computational complexity of our BP identification scheme using SpaRSA is moderate, and adapting it for real-time operation seems to be within reach.

ACKNOWLEDGMENT

This work was supported by Fundação para a Ciência e a Tecnologia through project PTDC/EEA-TEL/71263/2006 (PHITOM) and ISR/IST plurianual funding.

REFERENCES

- [1] B. Li, S. Zhou, M. Stojanovic, L. Freitag, and P. Willett, "Multicarrier communication over underwater acoustic channels with nonuniform Doppler shifts," *IEEE J. Ocean. Eng.*, vol. 33, no. 2, pp. 198–209, Apr. 2008.
- [2] B. Li, J. Huang, S. Zhou, K. Ball, M. Stojanovic, L. Freitag, and P. Willett, "MIMO-OFDM for high rate underwater acoustic communications," *IEEE J. Ocean. Eng.*, vol. 34, no. 4, pp. 634–645, Oct. 2009.
- [3] G. Leus and P. van Walree, "Multiband OFDM for covert acoustic communications," *IEEE J. Sel. Areas Commun.*, vol. 26, no. 9, pp. 1662–1673, Dec. 2008.
- [4] S.-J. Hwang and P. Schniter, "Efficient multicarrier communication for highly spread underwater acoustic channels," *IEEE J. Sel. Areas Commun.*, vol. 26, no. 9, pp. 1674–1683, Dec. 2008.
- [5] D. Kilfoyle and A. Baggeroer, "The state of the art in underwater acoustic telemetry," *IEEE J. Ocean. Eng.*, vol. 25, no. 1, pp. 4–27, Jan. 2000.
- [6] P. Schniter, "Low-complexity equalization of OFDM in doubly selective channels," *IEEE Trans. Signal Process.*, vol. 52, no. 4, pp. 1002–1011, Apr. 2004.
- [7] L. Rugini, P. Banelli, and G. Leus, "Low-complexity banded equalizers for OFDM systems in Doppler spread channels," *EURASIP J. Appl. Signal Process.*, vol. 2006, Article ID 67404, pp. 1–13, 2006.
- [8] D. Dowling, "Acoustic pulse compression using passive phase-conjugate processing," *J. Acoust. Soc. Am.*, vol. 95, no. 3, pp. 1450–1458, Mar. 1994.
- [9] J. Gomes, A. Silva, and S. Jesus, "Experimental assessment of time-reversed OFDM underwater communications," in *Proc. Acoustics'08*, Paris, France, June 2008.
- [10] —, "OFDM demodulation in underwater time-reversed shortened channels," in *Proc. MTS/IEEE OCEANS'08*, Quebec City, Canada, Sept. 2008.
- [11] —, "Adaptive spatial combining for passive time-reversed communications," *J. Acoust. Soc. Am.*, vol. 124, no. 2, pp. 1038–1053, Aug. 2008.
- [12] A. Bruckstein, D. Donoho, and M. Elad, "From sparse solutions of systems of equations to sparse modeling of signals and images," *SIAM Review*, vol. 51, no. 1, pp. 34–81, Feb. 2009.
- [13] W. Bajwa, J. Haupt, A. Sayeed, and R. Nowak, "Compressed channel sensing: A new approach to estimating sparse multipath channels," *Proc. IEEE*, vol. 98, no. 6, pp. 1058–1076, June 2010.
- [14] G. Tauböck, F. Hlawatsch, D. Eiwen, and H. Rauh, "Compressive estimation of doubly selective channels in multicarrier systems: Leakage effects and sparsity-enhancing processing," *IEEE J. Sel. Topics. Signal Process.*, vol. 4, no. 2, pp. 255–271, Apr. 2010.
- [15] C. R. Berger, S. Zhou, J. Preisig, and P. Willett, "Sparse channel estimation for multicarrier underwater acoustic communication: From subspace methods to compressed sensing," *IEEE Trans. Signal Process.*, vol. 58, no. 3, pp. 1708–1721, Mar. 2010.
- [16] M. Stojanovic, "Efficient processing of acoustic signals for high rate information transmission over sparse underwater channels," *Elsevier J. Physical Commun.*, vol. 1, no. 2, pp. 146–161, June 2008.
- [17] —, "OFDM for underwater acoustic communications: Adaptive synchronization and sparse channel estimation," in *Proc. Int. Conf. Acoust., Speech, Signal Process. (ICASSP'08)*, Las Vegas, USA, Mar. 2008.
- [18] S. Wright, R. Nowak, and M. Figueiredo, "Sparse reconstruction by separable approximation," *IEEE Trans. Signal Process.*, vol. 57, no. 7, pp. 2479–2493, July 2009.
- [19] J.-Z. Huang, C. R. Berger, S. Zhou, and J. Huang, "Comparison of basis pursuit algorithms for sparse channel estimation in underwater acoustic OFDM," in *Proc. MTS/IEEE OCEANS'10*, Sydney, Australia, May 2010.
- [20] J. Proakis and M. Salehi, *Digital Communications*, 5th ed. McGraw-Hill, 2007.
- [21] P. Carrasco and M. Stojanovic, "Adaptive channel estimation and data detection for underwater acoustic MIMO-OFDM systems," *IEEE J. Ocean. Eng.*, vol. 35, no. 3, pp. 635–646, July 2010.
- [22] B. Sharif, J. Neasham, O. Hinton, and A. Adams, "A computationally efficient Doppler compensation system for underwater acoustic communications," *IEEE J. Ocean. Eng.*, vol. 25, no. 1, pp. 52–61, Jan. 2000.
- [23] H. Song, W. Hodgkiss, W. Kuperman, W. Higley, K. Raghukumar, T. Akal, and M. Stevenson, "Spatial diversity in passive time reversal communications," *J. Acoust. Soc. Am.*, vol. 120, no. 4, pp. 2067–2076, Oct. 2006.